

Characterization of Primary and Secondary Malignant Liver Lesions from B-Mode Ultrasound

Jitendra Virmani · Vinod Kumar · Naveen Kalra ·
Niranjan Khandelwal

Published online: 15 February 2013
© Society for Imaging Informatics in Medicine 2013

Abstract Characterization of hepatocellular carcinomas (HCCs) and metastatic carcinomas (METs) from B-mode ultrasound presents a daunting challenge for radiologists due to their highly overlapping appearances. The differential diagnosis between HCCs and METs is often carried out by observing the texture of regions inside the lesion and the texture of background liver on which the lesion has evolved. The present study investigates the contribution made by texture patterns of regions inside and outside of the lesions for binary classification between HCC and MET lesions. The study is performed on 51 real ultrasound liver images with 54 malignant lesions, i.e., 27 images with 27 solitary HCCs (13 small HCCs and 14 large HCCs) and 24 images with 27 MET lesions (12 typical cases and 15 atypical cases). A total of 120 within-lesion regions of interest and 54 surrounding lesion regions of interest are cropped from 54 lesions. Subsequently, 112 texture features (56 texture features and 56 texture ratio features) are computed by statistical, spectral, and spatial filtering based texture features extraction methods. A two-step methodology is used

for feature set optimization, i.e., feature pruning by removal of nondiscriminatory features followed by feature selection by genetic algorithm–support vector machine (SVM) approach. The SVM classifier is designed based on optimum features. The proposed computer-aided diagnostic system achieved the overall classification accuracy of 91.6 % with sensitivity of 90 % and 93.3 % for HCCs and METs, respectively. The promising results obtained by the proposed system indicate its usefulness to assist radiologists in diagnosing liver malignancies.

Keywords Texture analysis · B-Mode liver ultrasound · Hepatocellular carcinoma · Metastasis · Primary malignant liver lesion · Secondary malignant liver lesion · Genetic algorithm · Support vector machine classifier · Small hepatocellular carcinoma · Large hepatocellular carcinoma · Typical metastasis · Atypical metastasis · Focal liver lesions

Introduction

The real-time imaging capabilities offered by widely available ultrasound (US) imaging modality along with its inexpensive, nonradioactive, and noninvasive nature makes it a first-line examination for screening of focal liver lesions (FLLs) [1, 2]. However, there are certain disadvantages associated with the use of conventional gray-scale US for characterization of FLLs. (1) There is limited sensitivity for detection of small FLLs (<2 cm) developed on cirrhotic liver which is already nodular and coarse-textured [3–5]. (2) Sonographic appearance of hepatocellular carcinoma (HCC), primary malignant solid FLL and metastatic carcinoma (MET), secondary malignant solid FLL are highly overlapping [1, 3–6].

The sensitivity of contrast-enhanced US, contrast-enhanced spiral computed tomography, and magnetic resonance imaging modalities for detection and characterization

J. Virmani (✉)
Biomedical Instrumentation Laboratory, Department of Electrical Engineering, Indian Institute of Technology Roorkee, Uttarakhand 247667, India
e-mail: jitendra.virmani@gmail.com

V. Kumar
Department of Electrical Engineering, Indian Institute of Technology Roorkee, Uttarakhand 247667, India
e-mail: vinodfee@gmail.com

N. Kalra · N. Khandelwal
Department of Radiodiagnosis and Imaging, Post Graduate Institute of Medical Education and Research, Sector-12, Chandigarh 160012, India

N. Kalra
e-mail: navkal2004@yahoo.com

N. Khandelwal
e-mail: khandelwaln@hotmail.com

of FLLs is higher than conventional gray-scale US, but these modalities are not widely available, expensive, and pose greater operational inconvenience [1, 3–6]. Therefore, a computer-aided diagnostic (CAD) system for accurate characterization of primary and secondary malignant FLLs based on conventional gray-scale US is highly desired to facilitate radiologists in clinical environment.

Among malignant FLLs, the present study is focused on characterization of HCC (most common primary malignant FLL) and MET (most common secondary malignant FLL). For the present work, benign FLLs such as hemangioma (HEM) and cyst are not considered because experienced participating radiologists (co-authors of this paper) having 13 and 23 years of experience in US imaging opined that HEM and cysts can be easily diagnosed from B-mode US with their classic diagnostic features. Typically, HEM appears as a well-circumscribed and uniformly hyperechoic lesion and cyst appears as a well-defined, rounded, anechoic lesion with thin imperceptible walls and posterior acoustic enhancement [1, 4, 5]. These typical sonographic appearances of benign FLLs can easily be differentiated from malignant FLLs, but differentiation between HCC and MET malignant lesions presents a daunting challenge even for experienced radiologists.

Early and accurate characterization of malignant FLLs is necessary because treatment options like curative surgical resection or successful percutaneous ablation are only possible if these malignancies are detected early [3, 5]. However, the practical problem faced by radiologists during routine practice is highly overlapping sonographic appearances of HCC (small and large HCCs on top of cirrhosis) and MET lesions (atypical METs) [1, 4, 5].

In 85 % of cases, HCC occurs in patients with cirrhosis. In fact in radiology practice, the condition of cirrhosis is seen as a precursor to the development of HCC [1, 3–5]. The only feature which favors the possibility of HCC in differential diagnosis between HCC and other FLLs is that HCC is most commonly associated with cirrhosis [1]. The sonographic appearances of small HCCs (<2 cm) vary from hypoechoic to hyperechoic. Large HCCs appear frequently with mixed echogenicity [4, 5]. A lesion can be labeled as typical in appearance when its subjective diagnosis can be made with a good confidence level by looking at the US examination. Experienced participating radiologists opined that the HCC case series should not be isolated as having typical or atypical sonographic appearance because of wide variability of sonographic appearances even within small and large HCCs; therefore, no sonographic appearance is typical for HCC. A representative dataset for designing the classifier should contain both small and large HCCs.

The occurrence rate of MET is 20 times more than that of HCC eventually because liver is the most common site for metastatic disease [5, 6]. Metastatic deposits may appear as single solitary mass or multiple masses of varying sizes. The sonographic appearance of MET lesions is extremely variable ranging from anechoic, hypoechoic, isoechoic, hyperechoic, and even with mixed echogenicity [1, 3–6]. However, the typical sonographic appearance of MET lesion is the “target” or “bull’s-eye” appearance (i.e., hypoechoic center surrounded by a hyperechoic rim) [1, 7, 8]. Diagnosis of these typical MET lesions can be made easily by an experienced radiologist from B-mode US, but differentiating atypical metastasis from HCCs lesions is considerably difficult. The sample images of small HCC, large HCC, typical MET, and atypical MET lesions from the acquired database are shown in Fig. 1.

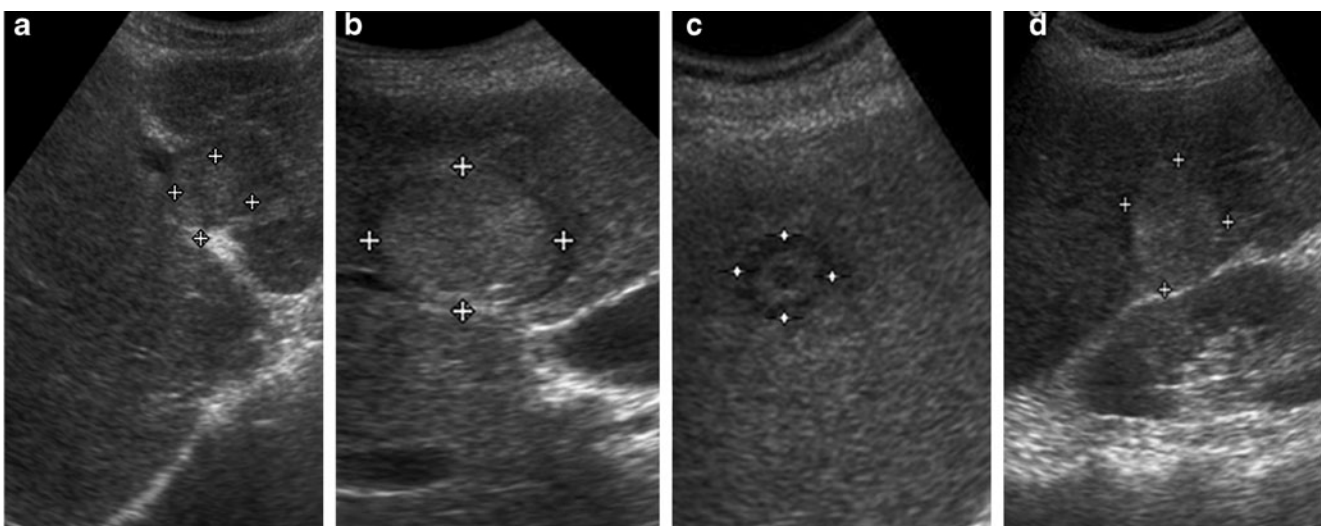


Fig. 1 Ultrasound liver images. **a** Small HCC image. **b** Large HCC image. **c** Typical MET image. **d** Atypical MET image. In (c), typical “bull’s-eye” appearance of MET lesion alternating layers of hyper- and hypoechoic tissue are clearly visible

The sonographic characterization of HCC and MET lesions is often carried out not only by observing the textural characteristics of regions inside the lesion but also by the texture of the background liver on which the lesion has evolved [1, 9]. The experienced participating radiologists opined that the textural characteristics of the neighboring liver parenchyma surrounding the lesion should contribute for differentiating the HCC and MET lesions from B-mode US. The present work investigates the contribution of texture of surrounding liver parenchyma in characterization of HCC and MET malignant liver lesions.

The related researches in literature for characterization of FLLs are few. The brief details of these studies [8, 10–12] are depicted in Table 1.

The study in [10] reported classification of benign, malignant, and normal liver with statistical texture analysis methods by using linear discriminant analysis and neural network classifier. The study in [12] reported classification of cyst, HEM, strike out this and malignant and normal liver with manually selected optimal statistical and spectral texture features by using a neural network classifier. A CAD system for classification in five classes, namely, HEM, cyst, HCC, MET, and normal liver, is proposed in [8]. However, their proposed CAD system is developed using a large feature vector consisting of 208 features extracted with statistical, spectral, and spatial filtering based methods and neural network classifiers. In studies [10, 12], malignant lesions are considered as single class; however, the characterization of malignant lesions as HCC or MET lesions is clinically significant for effective treatment and management of liver malignancies [3, 5]. The study in [8] used the region of interest (ROI) size of 25×25 pixels for computing texture features; however, in [10, 11] the use of ROI size of 10×10 pixels is reported. The use of 10×10 pixels and even 25×25 pixels as ROI size yields a smaller number of pixels in comparison to minimum 800 pixels required to estimate reliable statistics [13–15].

The related research reported in [12] used wavelet packet texture descriptors with neural network classifier for binary classification tasks, i.e., HEM vs. HCC, HEM vs. MET, and HCC vs. MET. Among these, the lowest characterization performance for HCC vs. MET is reported on their data. Their study reports the use of 64×64 pixels as ROI size, possibly because they used high-resolution scanned images instead of real US images. It is otherwise difficult to select such a large ROI size keeping in view the size of small lesions and resolution of images obtained from US machines.

According to the best of the authors' knowledge, all the researches in literature for characterization of FLLs have considered only the texture patterns of regions inside the lesions, and a CAD system for characterization of HCC and MET lesions has not been experimented as yet. The present study investigates the contribution made by texture patterns

of regions inside and outside of the lesions for binary classification of HCC and MET lesions.

In the present work, support vector machine (SVM) has been chosen for the classification task because classifier designs which use regularization like SVM are less prone to overfitting and obtain good generalization performance to a certain extent even without feature space dimensionality reduction [16–18]. Extensive literature surveys on texture classification reveal that SVM has shown remarkable performance for classification of medical images [19–27].

Materials and Methods

Data Collection and Description

Data Collection For the present work, 51 images were collected from 51 different patients; out of these 27 images are HCC images with 27 solitary HCC lesions and 24 images are MET images with 27 MET lesions, i.e., 21 MET images with solitary MET lesion and 3 MET images with 2 MET lesions each. These images were collected from different patients visiting the Department of Radiodiagnosis and Imaging, Post Graduate Institute of Medical Education and Research (PGIMER), Chandigarh, India over the time period from March 2010 to December 2011. Informed consent of patients for using these images for research was taken prior to recording. The medical ethics board of PGIMER, Chandigarh, granted the ethical clearance to carry out this research work. The direct digital images recorded by using Philips ATL HDI 5000 US machine equipped with multifrequency transducer of 2–5 MHz range were used. The size of the images is 800×564 pixels with gray scale consisting of 256 tones, and horizontal as well as vertical resolution is 96 dpi. The following protocols were followed for data collection:

- (1) The judgment regarding the diagnostic quality (free from artifacts) and representativeness of each image class (HCC and MET) was made by two domain experts (co-authors of this paper) with 13 and 23 years of experience in US imaging.
- (2) The acquired dataset contained 27 HCC images with 27 solitary HCC lesions comprising of 13 small HCC lesions and 14 large HCC lesions. While recording these images, both transverse and longitudinal views of each image were observed to determine the size of each lesion. (The HCC lesion was considered as small if its size was less than or equal to 2 cm.)
- (3) Only HCCs evolved on cirrhotic liver are considered.
- (4) The acquired dataset contained 24 MET images with 27 metastatic lesions comprising of 12 lesions with typical bull's-eye or target appearance and 15 MET lesions with variable sonographic appearances.
- (5) The labeling of HCC lesions as small HCC and

Table 1 Studies on classification of FLLs

Authors (year)	Liver image classes	Dataset description				
		Patients	Images per class	No. of ROIs	ROI size	
Sujana et al. (1996) [10]	NOR	–	–	113	10 × 10 pixels	
	HEM					
	Malignant					
	Classifier used Neural Network LDA	Distribution of ROIs for classifier design		Testing data		
		NOR (40)		NOR (13)		
		HEM (15)		HEM (5)		
		Malignant (30)		Malignant (10)		
Yoshida et al. (2003) [12]	HEM	44	HEM (17)	193	64 × 64 pixels	
	Malignant (HCC+MET)		HCC (11)			
			MET (16)			
	Classifier used Neural Network	Cross-validation procedure				
		HEM (50)				
		HCC (87)				
		MET (56)				
Poonguzhali et al. (2008) [11]	NOR	–	–	120	10 × 10 pixels	
	Cyst					
	HEM					
	Malignant					
	Classifier used Neural Network	Cross-validation procedure				
		NOR (30)				
		Cyst (30)				
		HEM (30)				
		Malignant (30)				
Mittal et al. (2011) [8]	NOR	88	NOR (16)	800	25 × 25 pixels	
	Cyst		Cyst (17)			
	HEM		HEM (18)			
	HCC, MET		HCC (15)			
		MET (45)				
		Classifier used Neural Network	Training data		Validation data	Testing data
			NOR (50)		NOR (10)	NOR (172)
			Cyst (50)		Cyst (10)	Cyst (6)
		HEM (50)		HEM (10)	HEM (30)	
		HCC (50)		HCC (10)	HCC (167)	
		MET (50)		MET (10)	MET (125)	
Present study (2013)	HCC	51	HCC (27)	174 (120 WLROIs, 54 SLROIs)	32 × 32 pixels	
	MET		MET (24)			
		Classifier used	Training data		Testing data	
		SVM	HCC (30)		HCC (30)	
		MET (30)		MET (30)		

In the present work, HCCs evolved on cirrhotic liver are considered
WLROIs within-lesion ROIs, *SLROIs* surrounding lesion ROIs, *SVM* support vector machine

large HCC lesions and labeling of MET lesions as one with typical target bull’s-eye appearance and other atypical sonographic appearances was done during data collection solely for the purpose of having representative data in training set for designing the classifier.

Selection of Regions of Interest (ROIs) The following protocols were followed for cropping the ROIs from the image database (cropping here refers to extraction of ROIs not to be confused with similar terminology used in photography for removal of unwanted details/objects in the images):

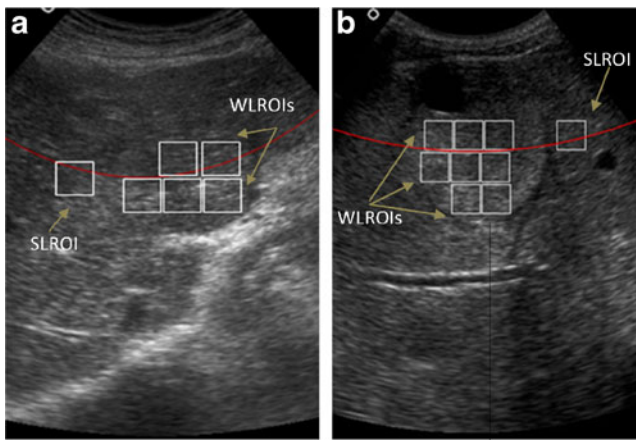


Fig. 2 **a** HCC image with WLROIs and SLROI marked. **b** MET image with WLROIs and SLROI marked. Necrotic area within the MET lesion is avoided while cropping WLROIs

(1) The ROIs were cropped by an experienced participating radiologist by using a specially designed ROI manager

software developed in Biomedical Instrumentation Laboratory, Indian Institute of Technology, Roorkee. This ROI manager software provided the radiologist the flexibility to load the image, choose the ROI size and shape, move the ROI to any desired location over the image, freeze the ROI at any location, and crop the ROIs together after the position of all the ROIs for a particular image is frozen. (2) Two types of ROIs are used in this study, within-lesion ROIs (WLROIs) and surrounding lesion ROIs (SLROIs). (3) Maximum nonoverlapping WLROIs were cropped from well within the boundary of each lesion. (4) The areas of necrosis were avoided while cropping WLROIs. (5) For each lesion, a single SLROI was cropped approximately at the same depth as that of the center of the lesion. (6) SLROI were cropped by avoiding the inhomogeneous structures like hepatic ducts and blood vessels, etc.

In the present work, two types of features are considered for analysis, i.e., texture features computed from WLROIs and texture ratio features computed by taking the ratio of

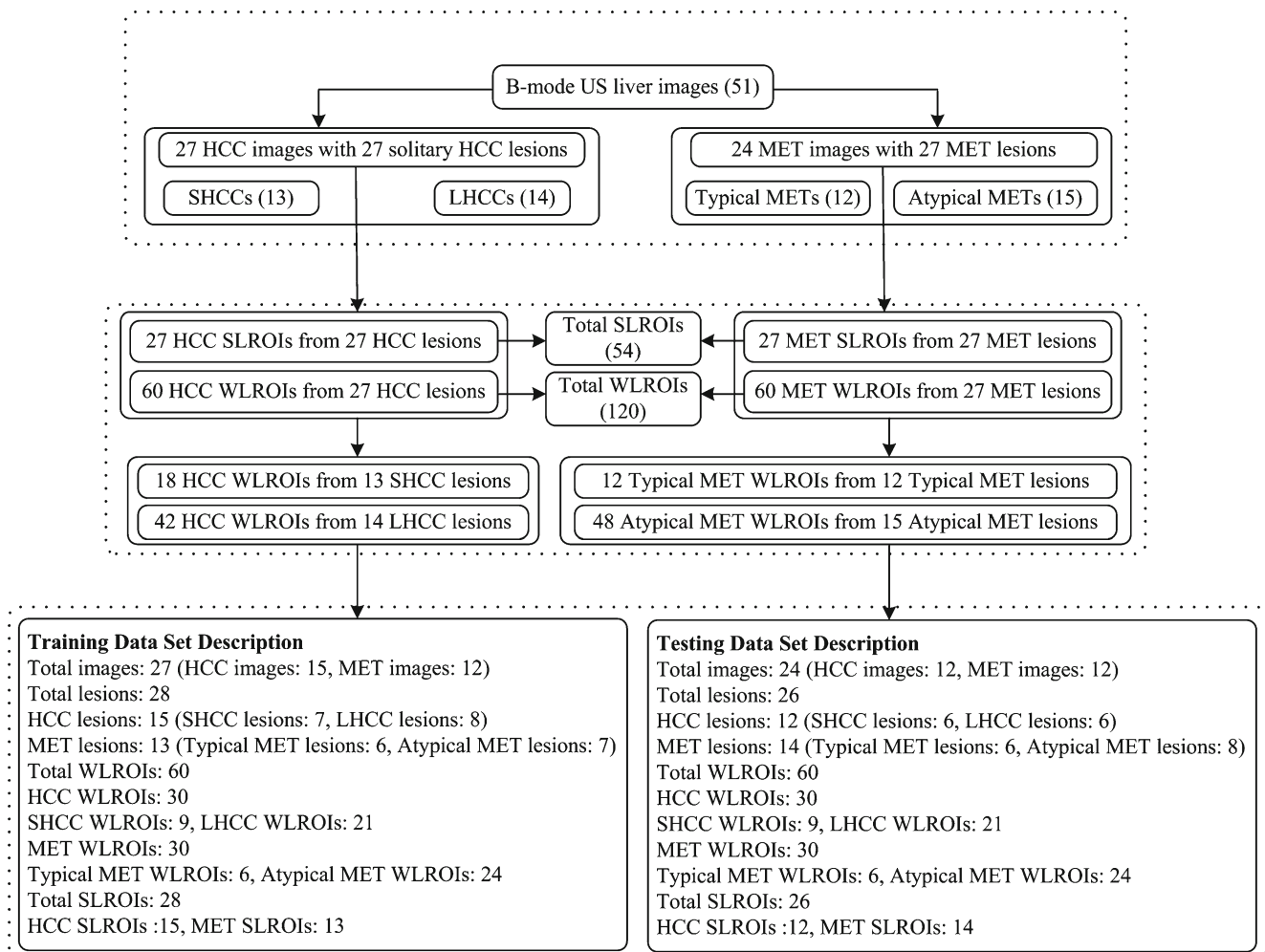


Fig. 3 Data set description. The size of small HCC lesion varied from 1.5 to 1.9 cm, size of large HCC lesion varied from 2.1 to 5.6 cm, and size of MET lesion varied from 1.1 to 6.8 cm

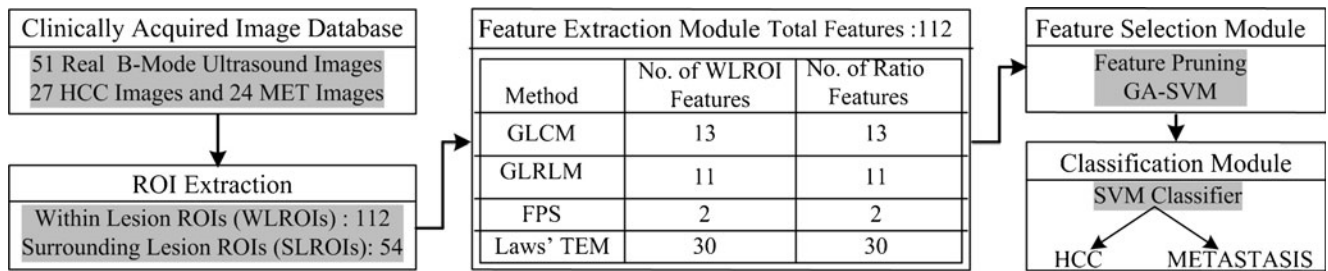


Fig. 4 CAD system for characterization of malignant FLLs

texture feature computed from WLROI and texture feature computed from corresponding SLROI.

It can be noted that HCC lesion in Fig. 2a contains five WLROIs and a corresponding SLROI. Thus, five instances of a single texture feature can be obtained with these five WLROIs and five instances of texture ratio feature can be obtained by dividing the texture feature value obtained for each WLROI with the texture feature value obtained for the corresponding SLROI.

Selection of ROI Size The ROI size should be chosen so as to provide good statistical population for computing texture features. In literature, different ROI sizes ranging from 10 × 10 pixels [9, 11], 25 × 25 pixels [8], and 64 × 64 pixels [12] have been chosen for classification of FLLs. After interaction with the participating radiologists, ROI size of 32 × 32 pixels was considered appropriate for the present study considering the facts mentioned below:

1. There is sufficient evidence in the literature that ROI size must be at least 800 pixels to provide good sampling distribution for estimating reliable statistics [13–15]; as ROI size of 32 × 32 gives 1,024 pixels, it can be believed that the computed texture parameters are reliable estimates.
2. During initial discussions with the participating radiologists, an attempt was made to mark larger ROI sizes, but few practical difficulties were faced. Certain lesions had necrotic area, radiologists opined that the necrotic area inside lesions must be avoided while extracting WLROIs, and it was not possible to consider large ROI size for these lesions. Also, participating radiologists were of the view that SLROI for each lesion must be selected by avoiding the inhomogeneous structures like hepatic ducts and blood vessels, etc., which was practically difficult by considering larger ROI size.
3. For real-time implementation, small ROI size is always favorable as time taken for feature extraction and classification is obviously less in comparison to large ROI size. Also, with small ROI size, more number of samples are available for classifier design.

Interpretation by Radiologists One of the experienced participating radiologist having more than 13 years of experience

confirmed the presence of HCC and MET lesions using liver image assessment criteria including (1) visualization of sonographic appearances, imaging features of FLLs based on their knowledge and expertise, (2) follow-up of clinical history of the patient and other associated findings, and (3) imaging appearance on dynamic helical computed tomography (CT)/magnetic resonance imaging (MRI)/pathological examinations and biopsy, which is an invasive procedure.

Data Set Description The distribution of clinically acquired database of 51 B-mode liver US images among HCC and MET image categories and the bifurcation of ROIs in training and test data set is described in Fig. 3 below.

Proposed Computer-Aided Diagnostic System The block diagram of the proposed CAD system is depicted in Fig. 4.

For implementation of the proposed CAD system, the database of 120 nonoverlapping WLROIs and 54 SLROIs was created from 51 clinically acquired US images. The CAD system consisted of feature extraction, feature selection, and classification modules. In feature extraction module, texture features are computed from WLROIs as well as SLROIs by gray-level co-occurrence matrix (GLCM) [28], gray-level run length matrix (GLRLM) [29–31], Fourier power spectrum (FPS) [32], and Laws’ texture feature [33] extraction methods. In feature selection module, initially feature pruning is carried out by removal of nondiscriminatory feature vectors followed by feature selection by genetic algorithm–support vector machine (GA–SVM) approach. The GA–SVM procedure results in optimal reduced set

L7L7	E7L7	S7L7
L7E7	E7E7	S7E7
L7S7	E7S7	S7S7

Fig. 5 Nine 2-D Laws’ masks

of features. In classification module, a support vector machine (SVM) classifier is designed with the selected optimal features. The SVM classifier is implemented using LibSVM library [34].

Feature Extraction The general idea of feature extraction is to convert both visually extractable and visually non-extractable sonographic features into mathematical descriptors. These mathematical descriptors are either morphological (based on shape or contour of the lesion) or textural features (based on intensity distribution) [35]. Both these morphological as well as textural features are significant for developing CAD systems for breast lesions from B-mode US [36–39]. Experienced participating radiologists opined that morphological sonographic features of FLLs do not give any significant information for their characterization; as also evident from other related researches, the proposed CAD systems for characterization of FLLs from B-mode US have relied on textural features only [8, 10–12].

Initially, a wide variety of visual and nonvisual echotexture features are extracted by using statistical, spectral, and spatial filtering based feature extraction methods. These features are then applied in the present classification system with a tedious

task of combining the most relevant and effective features while discarding the nonperforming features.

Statistical texture features are defined by the spatial distribution of gray-level intensity values in the image. Local features are computed at each point in the image and a set of statistics are derived from the distribution of these local features. Statistical methods are classified as first-order statistics, second-order statistics, or higher-order statistics depending upon the number of pixels used in defining a local feature [8, 40].

Spectral features computed by FPS method such as radial sum and angular sum of the discrete Fourier transform are used to describe texture [32].

Spatial filtering based texture descriptors, i.e., Laws' texture features, determine texture properties by performing local averaging, edge detection, spot detection, wave detection, and ripple detection in texture [33]. Laws' texture features are computed by using special 1-D filters of length 3, 5, 7, and 9. Different filter lengths correspond to different resolutions for extraction of texture features from a ROI. In the present work, 1-D filters of length 7, i.e., $L7 = [1, 1, 6, 6, 15, 15, 20]$, $E7 = [-1, -4, -5, 0, 5, 4, 1]$, and $S7 = [-1, -2, 1, 4, 1, -2, -1]$, are used. Special 2-D filters called Laws' masks are derived by outer vector product of these 1-D kernels with themselves or with each other as shown in Fig. 5.

Table 2 Description of 112 texture features extracted for characterizing HCC and MET FLLs

Statistical methods		Spectral method	Spatial filtering method	
GLCM features (13)	GLRLM features (11)	FPS features (2)	Laws' texture features (30)	
F1: angular second moment	F14: short run emphasis	F25: angular sum	F27: LLmean	F45: LLkurt
F2: contrast	F15: long run emphasis	F26: radial sum	F28: EEmean	F46: EEkurt
F3: correlation	F16: low gray level run emphasis		F29: SSmean	F47: SSkurt
F4: sum of squares variance	F17: high gray level run emphasis		F30: LEmean	F48: LEkurt
F5: inverse difference moment	F18: short run low gray level emphasis		F31: LSmean	F49: LSkurt
F6: sum average	F19: short run high gray level emphasis		F32: ESmean	F50: ESkurt
F7: sum variance	F20: long run low gray level emphasis		F33: LLstd	F51: LLenergy
F8: sum entropy	F21: long run high gray level emphasis		F34: EEstd	F52: EEenergy
F9: entropy	F22: gray level non uniformity		F35: SSstd	F53: SSenergy
F10: difference variance	F23: run length non uniformity		F36: LEstd	F54: LEenergy
F11: difference entropy	F24: run percentage		F37: LSstd	F55: LSenergy
F12: information measures of correlation—1			F38: ESstd	F56: ESenergy
F13: information measures of correlation—2			F39: LLskew	
			F40: EEskew	
			F41: SSskew	
			F42: LEskew	
			F43: LSskew	
			F44: ESSkew	
F57 to F112: 56 texture ratio features corresponding to above features (F1 to F56). [Note: the above 56 features (F1 to F56) are computed for each WLROI and SLROI so as to compute another 56 texture ratio features (F57 to F112) corresponding to the above features]				
F57–69: GLCM ratio features (13)	F70–F80: GLRLM ratio features (11)	F81–82: FPS ratio features (2)	F83–F112: Laws' ratio features (30)	

The texture images are obtained by convolving the ROI of size $M \times N$ with these 2D Laws’ masks, for example

$$TI_{E7E7} = ROI \otimes E7E7 \tag{1}$$

The output TIs are processed by texture energy measurement (TEM) filters. The TEM filter performs moving average nonlinear filtering operation as depicted by:

$$TEI = TEM[TI(x, y)] = \sum_{i=-7}^7 \sum_{j=-7}^7 |I(x + i, y + j)| \tag{2}$$

Here, 15×15 descriptor windows are used to obtain nine texture energy images (TEIs). Texture energy images obtained by a pair of identical filters, for example, TEI_{E7L7} and TEI_{L7E7} , are combined to obtain a rotational invariant image (90° rotational invariance) (TR) [41].

$$TR_{E7L7} = \frac{TEI_{E7L7} + TEI_{L7E7}}{2} \tag{3}$$

Statistics derived from these TR images provide significant texture information of ROI. Five statistics, i.e., mean, standard deviation, skewness, kurtosis, and energy are extracted from each TR image [41, 42]. Thus, 30 Laws’ texture features (6 TR images \times 5 statistical parameters) are computed for each ROI.

In the present work, statistical methods, i.e., GLCM and GLRLM methods, spectral method, i.e., FPS method, and spatial filtering based method, i.e., Laws’ texture feature extraction method, are selected for the classification task. The selection of these methods for the classification task is based on other related researches with US images [13, 14, 41, 43] and few other studies for diagnosis of FLLs with US images [8, 10–12].

For extraction of efficient diagnostic features for characterization of liver malignancies, initially 112 features (56 features computed from WLROIs and 56 texture ratio features) are computed using GLCM, GLRLM, FPS, and Laws’ texture feature extraction methods as tabulated in Table 2.

For computation of Laws’ texture features, different 1-D filters of length 5, 7, and 9 were experimented as shown in Table 3.

Statistics derived from TRs are used as feature vectors. In the present work, five features, i.e., mean, standard deviation, skewness, kurtosis, and energy, are computed from TRs. Thus, feature vector of lengths 70, 30, and 70 are obtained with 1-D filter of length 5, 7, and 9, respectively. It was observed that the classification accuracy obtained by SVM classifier by feature vector of length 30 obtained for filter length 7 is higher in comparison with feature vectors of length 70 obtained for filter lengths 5 and 9. Thus, 30 Laws’ texture features computed for filter length 7 are considered for further analysis.

Feature Selection Feature selection is used to eliminate the interference of irrelevant features which often increases the time taken to perform classification task and also reduces the classification accuracy. In the present work, two-step methodology is followed for feature selection. In the first step, initial feature pruning is carried out by removal of nondiscriminatory individual texture feature vectors (TFVs). The discrimination ability of a TFV is measured by the classification accuracy obtained by SVM classifier. Feature pruning yields a pruned TFV consisting of best-performing individual TFVs.

In the second step, GA–SVM feature selection is applied on pruned TFV; here binary genetic algorithm (GA) is used

Table 3 Description of various 1-D filters used for computation of Laws’ texture features

Length of 1-D filter	1-D filter coefficients	No. of 2-D Laws’ masks (X)	TRs obtained from identical filters pairs (Y)	Total TRs (X–Y)
5	L5=[1, 4, 6, 4, 1]	25	10	15
	E5=[-1, -2, 0, 2, 1]			
	S5=[-1, 0, 2, 0, -1]			
	W5=[-1, 2, 0, -2, 1]			
	R5=[1, -4, 6, -4, 1]			
7	L7=[1, 6, 15, 20, 15, 6, 1]	9	3	6
	E7=[-1, -4, -5, 0, 5, 4, 1]			
	S7=[-1, -2, 1, 4, 1, -2, -1]			
9	L9=[1, 8, 28, 56, 70, 56, 28, 8, 1]	25	10	15
	E9=[1, 4, 4, -4, -10, -4, 4, 4, 1]			
	S9=[1, 0, -4, 0, 6, 0, -4, 0, 1]			
	W9=[1, -4, 4, 4, -10, 4, 4, -4, 1]			
	R9=[1, -8, 28, -56, 70, -56, 28, -8, 1]			

TRs rotational invariant texture images

Table 4 Comparison of performance of SVM classifiers for various individual TFVs

Classification performance SVMs						
TFV (<i>l</i>)	CM		Accuracy (%)	Sen. _{HCC} (%)	Sen. _{MET} (%)	
GLCM features WLROIs (13)	H	H 16	M 14	58.3	53.3	63.3
	M	11	19			
GLCM ratio features (13)		20	10	70	66.6	73.3
GLRLM features WLROIs (11)		8	22	56.6	66.6	46.6
		20	10			
GLRLM ratio features (11)		22	8	71.6	73.3	70
FPS features WLROIs (2)		9	21	68.3	53.3	83.3
		16	14			
FPS ratio features (2)		5	25	53.3	56.6	50
		17	13			
Laws' features WLROIs (30)		15	15	70	86.6	53.3
		26	4			
Laws' ratio features (30)		14	16	56.6	66.6	46.6
		H	M			
		20	10			
		16	14			

Best-performing individual TFVs are in bold

TFV texture feature vector, *l* length of feature vector, CM confusion matrix, *H* HCC, *M* MET, *Sen._{HCC}* sensitivity for HCC cases, *Sen._{MET}* sensitivity for MET cases

Here, Sensitivity of class A, denoted as *Sen._A* refers to (Number of cases correctly classified as class A/ Total number of cases in class A)

to evolve subsets of pruned TFV and the classification accuracy obtained by the SVM classifier is used as a fitness function. The GA–SVM feature selection procedure removes irrelevant features from pruned TFV to yield an optimal subset of discriminatory features. The main steps for implementation of binary GA [39] are:

- Step 1 Define fitness function and select GA run parameters like population size, crossover type, crossover rate, and mutation rate.
- Step 2 Create initial population (a set of binary coded chromosomes or genotypes).
- Step 3 Decode chromosomes (binary chromosomes are converted into candidate solutions or phenotypes).

- Step 4 Fitness function (fitness evaluation of each candidate solution or phenotype).
- Step 5 Selection (the selection of parents to enter the mating pool based on fitness evaluation).
- Step 6 Applying crossover and mutation to generate offsprings
- Step 7 Create next generation (by evaluating offsprings using fitness function)

The GA terminates when there is no improvement in the fitness value or after a fixed number of successive iterations. In the present work, single-point crossover is used and the other run parameters are set as crossover rate equal to 0.7, mutation rate equal to 0.05, and population size equal to 20 after a series of trials.

Table 5 Performance of SVM classifier for combined TFV of all 56 WLROI texture features

Classification performance SVM							
TFV (<i>l</i>)	CM		Accuracy (%)	Sen. _{HCC} (%)	Sen. _{MET} (%)		
GLCM , GLRLM, FPS and Laws' texture features WLROIs (56)		H	M	61.6	60	63.3	
		H	18				12
		M	11				19

TFV texture feature vector, *l* length of feature vector, CM confusion matrix, *H* HCC, *M* MET, *Sen._{HCC}* sensitivity for HCC cases, *Sen._{MET}* sensitivity for MET cases

Here, Sensitivity of class A, denoted as *Sen._A* refers to (Number of cases correctly classified as class A/ Total number of cases in class A)

Table 6 Performance of SVM classifier for combined TFV of all 56 texture ratio features

Classification performance SVM						
TFV (<i>l</i>)	CM			Accuracy (%)	Sen. _{HCC} (%)	Sen. _{MET} (%)
GLCM, GLRLM, FPS, and Laws' texture ratio features (56)	H	H	M	78.3	70	86.6
		21	9			
	M	4	26			

TFV texture feature vector, *l* length of feature vector, CM confusion matrix, *H* HCC, *M* MET, *Sen._{HCC}* sensitivity for HCC cases, *Sen._{MET}* sensitivity for MET cases

Here, Sensitivity of class A, denoted as *Sen._A* refers to (Number of cases correctly classified as class A/ Total number of cases in class A)

Classification

SVM Classifier The SVM classifier attempts to construct an optimum hyperplane in the higher dimensional feature space to separate the training data with minimum expected risk. Kernel functions are used for nonlinear mapping of the training data from input space to higher dimensional feature space. In the present work, the performance of Gaussian Radial Basis Function kernel is investigated. For a detailed description of SVM approach, additional information can be found in [16, 17].

A crucial step for obtaining good generalization performance is correct choice of the regularization parameter *C* and kernel parameter γ . The regularization parameter *C* attempts to maximize the margin while keeping low value for training error. In the present work, extensive search is carried out in the parameter space for the values of $C \in \{2^{-4}, 2^{-3} \dots 2^{15}\}$, $\gamma \in \{2^{-12}, 2^{-11} \dots 2^4\}$ using 10-fold cross-validation on training data. To avoid the bias caused by unbalanced feature values, the extracted features were normalized in the range [0, 1] by using min–max normalization procedure. For the present work, SVM classifier is implemented using LibSVM library [34].

Results

Rigorous experimentations were carried out to identify potential TFVs of texture features and texture ratio features for characterization of HCC and MET FLLs. In all the experiments, the

discrimination ability of texture feature vectors (TFVs) has been evaluated by using a SVM classifier.

In experiment 1, the discrimination ability of total 112 texture features, i.e., total eight TFVs (four TFVs corresponding to texture features and four TFVs corresponding to texture ratio features) obtained by GLCM, GLRLM, FPS, and Laws' feature extraction methods is investigated. The results of experiment 1 are used to obtain a pruned TFV by removal of individual nonperforming TFVs.

Experiments 2 and 3 investigate the discrimination ability of combined TFVs, i.e., combined TFV consisting of all texture features and combined TFV consisting of all texture ratio features. It is observed that combined TFV consisting of texture ratio features has more discrimination ability.

In experiment 4, the discrimination ability of pruned TFV obtained as a result of experiment 1 is examined. Experiment 5 investigates the discrimination ability of optimal reduced TFV obtained by passing pruned TFV to GA–SVM method.

Experiment 1 This experiment compares the performance of SVM classifiers by use of various individual TFVs. The results obtained are reported in Table 4. It can be seen from Table 4 that GLRLM texture ratio features provide highest classification accuracy of 71.6 %. Both Laws' WLROI features and GLCM ratio features provide the second highest accuracy of 70 %. It can also be observed that GLCM and GLRLM

Table 7 Performance of SVM classifier for pruned TFV

Classification performance SVM						
Feature vector (<i>l</i>)	CM			Accuracy (%)	Sen. _{HCC} (%)	Sen. _{MET} (%)
GLCM, GLRLM texture ratio features and FPS, Laws' features WLROIs (56)	H	H	M	80	76.6	83.3
		23	7			
	M	5	25			

TFV texture feature vector, *l* length of feature vector, CM confusion matrix, *H* HCC, *M* MET, *Sen._{HCC}* sensitivity for HCC cases, *Sen._{MET}* sensitivity for MET cases

Here, Sensitivity of class A, denoted as *Sen._A* refers to (Number of cases correctly classified as class A/ Total number of cases in class A)

Table 8 Performance of SVM classifier for optimal reduced TFV

Classification Performance SVM						
TFV (<i>l</i>)	CM			Accuracy (%)	Sen _{HCC} (%)	Sen _{MET} (%)
Texture ratio features WLROIs selected by GA–SVM method (9)	H	H	M	91.6	90	93.3
		27	3			
	M	2	28			

TFV texture feature vector, *l* length of feature vector, CM confusion matrix, *H* HCC, *M* MET, *Sen_{HCC}* sensitivity for HCC cases, *Sen_{MET}* sensitivity for MET cases

Here, Sensitivity of class A, denoted as *Sen_A* refers to (Number of cases correctly classified as class A/ Total number of cases in class A)

- ratio features show better characterization performance than corresponding WLROI features. Further, it can be noted that FPS and Laws' WLROI features show better characterization performance in comparison to corresponding ratio features.
- Experiment 2** This experiment evaluates the performance of SVM classifier by use of combined TFV of all 56 WLROI texture features. The results obtained are reported in Table 5. It can be seen from Table 5 that combined TFV of all 56 WLROI texture features provide a classification accuracy of 61.6 % for characterization of HCC and MET FLLs.
- Experiment 3** This experiment evaluates the performance of SVM classifier by use of combined TFV of all 56 texture ratio features. The results obtained are reported in Table 6. It can be seen from Table 6 that combined TFV of all texture ratio features provide classification accuracy of 78.3 %. For further experimentations, feature pruning is carried out on the basis of classification accuracy obtained by SVM classifier for eight individual TFVs shown in Table 4. The nonperforming individual TFVs are removed and the best-performing individual TFVs (highlighted in Table 4) are combined to form a pruned TFV for adequate discrimination of HCC and MET FLLs.
- Experiment 4** This experiment evaluates the performance of SVM classifier by use of pruned TFV of length 56 consisting of best-performing individual TFVs. The results obtained are reported in Table 7. From Table 7, it can be seen that pruned TFV yields a classification accuracy of 80 %. For further experimentation, this pruned TFV is subjected to GA–SVM feature selection procedure which iteratively removes the irrelevant and interfering features from the pruned TFV and returns an optimal reduced TFV of length 9. Nine texture features, i.e., four GLCM ratio features (angular second moment, sum average, difference entropy, and inverse difference moment), three GLRLM ratio features (long run emphasis, gray level non uniformity, and long run high gray level emphasis), one FPS WLROI feature (radial sum), and one Laws' WLROI feature (LLmean), are selected by GA–SVM procedure.

Table 9 Misclassification analysis of 60 cases of test data set

Misclassification analysis for HCC cases	Misclassification analysis for MET cases
Total HCC cases: 30	Total MET cases: 30
Small HCC cases: 9, large HCC cases: 21	Typical MET cases: 6, atypical MET cases: 24
Correctly classified: 27, misclassified: 3	Correctly classified: 28, misclassified: 2
Sensitivity HCC: 90 %	Sensitivity MET: 93.3 %
1 out of 9 small HCC cases is misclassified	All six typical MET cases are correctly classified
2 out of 21 large HCC cases are misclassified	2 out of 24 atypical MET cases are misclassified
Sensitivity _{SHCC} : 88.8 %	Sensitivity _{Typical MET} : 100 %,
Sensitivity _{LHCC} : 90.4 %	Sensitivity _{Atypical MET} : 91.6 %

Sensitivity_{SHCC} sensitivity for small HCC cases, *Sensitivity_{LHCC}* sensitivity for large HCC cases, *Sensitivity_{Typical MET}* sensitivity for typical MET cases, *Sensitivity_{Atypical MET}* sensitivity for atypical MET cases

Here, Sensitivity of class A, denoted as *Sen_A* refers to (Number of cases correctly classified as class A/ Total number of cases in class A)

Experiment 5 This experiment evaluates the performance of SVM classifier by use of optimal reduced TFV of length 9 consisting of features selected by GA–SVM procedure. The results obtained are reported in Table 8. From Table 8, it can be observed that using optimal reduced TFV consisting of nine features selected by GA–SVM procedure with SVM classifier yields the classification accuracy of 91.6 % and sensitivity of 90 % and 93.3 % for HCC and MET lesions, respectively. It is observed that for the studied population consisting of small HCCs, large HCCs, typical METs, and atypical METs, the proposed CAD system yields high sensitivity values for differentiation between malignant lesions. The generalization ability of the proposed CAD system can be tested by analyzing larger datasets.

Discussion

Misclassification Analysis Analysis of five misclassified cases out of 60 cases in the test data set is reported in Table 9. It can be observed from Table 9 that sensitivity of proposed CAD system for small HCC cases and large HCC cases is 88.8 % and 90.4 %, respectively. In case of MET cases, the sensitivity obtained is 100 % and 91.6 % for typical and atypical MET cases, respectively. However, it can be observed from Table 8 that the classification accuracy of the proposed CAD system is 91.6 % with sensitivity of 90 % for HCC cases and 93.3 % for MET cases. Given the fact that the sonographic appearances of HCC and MET overlap sufficiently, and the sensitivity of conventional B-mode US is limited, the results obtained by the proposed CAD system for the population studied are quite promising specifically in the presence of a comprehensive and representative dataset consisting of SHHCs, LHCCs, and typical as well as atypical MET cases. However, the generalization ability of the proposed CAD system remains to be tested by analyzing larger datasets for which data collection may take a long span of time. At the same time, it is worth mentioning that the selected features significantly account for the textural variations exhibited by primary and secondary liver malignancies as the proposed system performs well on unseen test data.

Conclusions

The ratio features are more discriminatory than WLROI features for characterization of HCC and MET FLLs. Only nine texture features (seven ratio features and two WLROI features) are significant to account for textural variations

exhibited by HCC and MET lesions. It can be concluded that the texture of the background liver on which the lesion has evolved do contribute towards characterization of primary and secondary malignant FLLs from B-mode US. The proposed CAD system yields the classification accuracy of 91.6 % with sensitivity of 90 % and 93.3 % for HCC and MET cases, respectively. The results obtained by the proposed CAD are up to the satisfaction of experienced participating radiologists. The promising results of the study indicate that the proposed CAD system can be routinely used in a clinical environment to assist radiologists in diagnosing liver malignancies and thereby facilitate in providing better disease management.

Acknowledgments The author Jitendra Virmani would like to acknowledge Ministry of Human Resource Development (MHRD), India for financial support. The authors wish to acknowledge the Department of Electrical Engineering, Indian Institute of Technology, Roorkee, India and Department of Radiodiagnosis and Imaging, Postgraduate Institute of Medical Education and Research, Chandigarh, India for their constant patronage and support in carrying out this research work. The authors would like to thank the anonymous reviewers for their substantive and informed review, which led to significant improvements in the manuscript.

References

1. Bates J: Abdominal Ultrasound How Why and When, 2nd edition. Churchill Livingstone, Oxford, 2004, pp 80–107
2. Virmani J, Kumar V, Kalra N, Khandelwal N: A rapid approach for prediction of liver cirrhosis based on first order statistics. In: Proceedings of IEEE International Conference on Multimedia, Signal Processing and Communication Technologies, IMPACT-2011, 212–215, 2011
3. Soye JA, Mullan CP, Porter S, Beattie H, Barltrop AH, Nelson WM: The use of contrast-enhanced ultrasound in the characterization of focal liver lesions. *Ulster Med J* 76(1):22–25, 2007
4. Colombo M, Ronchi G: Focal Liver Lesions—Detection, Characterization, Ablation. Springer, Berlin, 2005, pp 167–177
5. Harding J, Callaway M: Ultrasound of focal liver lesions. *Rad Magazine* 36(424):33–34, 2010
6. Jeffery RB, Ralls PW: Sonography of Abdomen. Raven, New York, 1995
7. Scheible W, Gossink BB, Leopold G: Gray scale echo graphic patterns of hepatic metastatic disease. *Am J Roentgenol* 129:983–987, 1977
8. Mittal D, Kumar V, Saxena SC, Khandelwal N, Kalra N: Neural network based focal liver lesion diagnosis using ultrasound images. *Int J Comput Med Imaging Graph* 35(4):315–323, 2011
9. Lee WL, Hsieh KS, Chen YC: A study of ultrasonic liver images classification with artificial neural networks based on fractal geometry and multiresolution analysis. *Biomed Eng Appl Basis Commun* 16(2):59–67, 2004
10. Sujana S, Swarnamani S, Suresh S: Application of artificial neural networks for the classification of liver lesions by image texture parameters. *Ultrasound Med Biol* 22(9):1177–1181, 1996
11. Poonguzhali S, Deepalakshmi, Ravindran G: Optimal feature selection and automatic classification of abnormal masses in ultrasound liver images. In: Proceedings of IEEE International Conference on Signal Processing, Communications and Networking, ICSCN'07, 503–506, 2007

12. Yoshida H, Casalino DD, Keserci B, Coskun A, Ozturk O, Savranlar A: Wavelet packet based texture analysis for differentiation between benign and malignant liver tumors in ultrasound images. *Phys Med Biol* 48:3735–3753, 2003
13. Kadah YM, Farag AA, Zurada JM, Badawi AM, Youssef AM: Classification algorithms for quantitative tissue characterization of diffuse liver disease from ultrasound images. *IEEE Trans Med Imaging* 15(4):466–478, 1996
14. Badawi AM, Derbala AS, Youssef ABM: Fuzzy logic algorithm for quantitative tissue characterization of diffuse liver diseases from ultrasound images. *Int J Med Inf* 55:135–147, 1999
15. Fukunaga K: *Introduction to Statistical Pattern Recognition*. Academic, New York, 1990
16. Burges CJC: A tutorial on support vector machines for pattern recognition. *Data Min Knowl Disc* 2(2):1–43, 1998
17. Guyon I, Weston J, Barnhill S, Vapnik V: Gene selection for cancer classification using support vector machines. *J Machine Learn* 46(1–3):1–39, 2002
18. Virmani J, Kumar V, Kalra N, Khandelwal N: SVM-based characterization of liver ultrasound images using wavelet packet texture descriptors. *J Digit Imaging*, 2012. doi:10.1007/s10278-012-9537-8
19. Wan J, Zhou S: Features extraction based on wavelet packet transform for b-mode ultrasound images. In: *Proceedings of IEEE International Congress on Image and Signal Processing, CISP-2010*, 949–955, 2010
20. Lee C, Chen S H: Gabor wavelets and SVM classifier for liver diseases classification from CT images. In: *Proceedings of IEEE International Conference on Systems, Man, and Cybernetics*, 548–552, 2006
21. Nawaz S, Dar A H: Hepatic lesions classification by ensemble of SVMs using statistical features based on co-occurrence matrix. In: *Proceedings of 4th IEEE International Conference on Emerging Technologies, ICET-2008*, 21–26, 2008
22. Huang YL, Chen DR, Jiang YR, Kuo J, Wu HK, Moon WK: Computer-aided diagnosis using morphological features for classifying breast lesions on ultrasound. *Ultrasound Obstet Gynecol* 32:565–572, 2008
23. Moayedi F, Azimifar Z, Boostani R, Katebi S: Contourlet based mammography mass classification. In: *Proceedings of ICIAR 2007, LNCS 4633*, 923–934, 2007
24. Huang YL, Wang KL, Chen DR: Diagnosis of breast tumors with ultrasonic texture analysis using support vector machines. *Neural Comput & Applic* 15:164–169, 2006
25. Reddy TK, Kumaravel N: A comparison of wavelet, curvelet and contourlet based texture classification algorithms for characterization of bone quality in dental CT. In: *Proceedings of International Conference on Environmental, Biomedical and Biotechnology, IPCBEE* 16:60–65, 2011
26. Tsiaparas N, Golemati S, Andreadis I, Stoitsis J: Multiscale geometric texture analysis of ultrasound images of carotid atherosclerosis. In: *Proceedings of 10th IEEE International Conference on Information Technology and Applications in Biomedicine, ITAB-2010*, 1–4, 2010
27. Minhas F, Sabih D, Hussain M: Automated classification of liver disorders using ultrasound images. *J Med Syst*, 2011. doi:10.1007/s10916-011-9803-1
28. Haralick R, Shanmugam K, Dinstein I: Textural features for image classification. *IEEE Trans Syst Man Cybern SMC-3(6)*:610–121, 1973
29. Galloway RMM: Texture analysis using gray level run lengths. *Comput Graphics Image Processing* 4:172–179, 1975
30. Chu A, Sehgal CM, Greenleaf JF: Use of gray value distribution of run lengths for texture analysis. *Pattern Recognition Lett* 11:415–420, 1990
31. Dasarathy BV, Holder EB: Image characterizations based on joint gray level-run length distributions. *Pattern Recognition Lett* 12:497–502, 1991
32. Weszka JS, Dyer CR, Rosenfeld A: A comparative study of texture measures for terrain classification. *IEEE Trans Syst Man Cybern SMC-6(4)*:269–285, 1976
33. Laws KI: Rapid texture identification. In: *SPIE Proceedings of the Seminar on Image Processing for Missile Guidance*. 238:376–380, 1980
34. Chang CC, Lin CJ: LIBSVM, a library of support vector machines. Software available at <http://www.csie.ntu.edu.tw/~cjlin/libsvm>. Accessed 15 June 2012
35. Kim SH, Lee JM, Kim KG, Kim JH, Lee JY, Han JK, Choi BI: Computer-aided image analysis of focal hepatic lesions in ultrasonography: preliminary results. *Abdom Imaging* 34(2):183–91, 2009
36. Huang YL, Chen DR, Jiang YR, Kuo SJ, Wu HK, Moon WK: Computer aided diagnosis using morphological features for classifying breast lesions on ultrasound. *Ultrasound Obstet Gynecol* 32:565–572, 2008
37. Moayedi F, Azimifar Z, Boostani R, Katebi S: Contourlet-based mammography mass classification. In: *Proceedings of 4th International Conference on Image Analysis and Recognition, ICIAR-2007, LNCS series (4633)*:923–934, 2007
38. Diao XF, Zhang XY, Wang TF, Chen SP, Yang Y, Zhong L: Highly sensitive computer aided diagnosis system for breast tumor based on color Doppler flow images. *J Med Syst* 35(5):801–809, 2011
39. Nandi RJ, Nandi AK, Rangayyan RM, Scutt D: Classification of breast masses in mammograms using genetic programming and feature selection. *Med Biol Eng Comput* 44(8):683–94, 2006
40. Srinivasan GN, Shobha G: Statistical texture analysis. *Proc World Acad Sci Eng Technol* 36:264–1269, 2008
41. Virmani J, Kumar V, Kalra N, Khandelwal N: Prediction of cirrhosis from liver ultrasound B-mode images based on Laws' masks analysis. In: *Proceedings of IEEE International Conference on Image Information Processing, ICIP-2011*, 1–5, 2011
42. Rachidi M, Marchadier A, Gadois C, Lespessailles E, Chappard C, Benhamou CL: Laws' masks descriptors applied to bone texture analysis: an innovative and discriminant tool in osteoporosis. *Skeletal Radiol* 37(6):541–548, 2008
43. Virmani J, Kumar V, Kalra N, Khandelwal N: Prediction of cirrhosis based on singular value decomposition of gray level co-occurrence matrix and a neural network classifier. In: *Proceedings of IEEE International Conference on Developments in E-systems Engineering, DeSe-2011*, 146–151, 2011